Received: 30 September 2025 | Revised: 22 January 2026 | Accepted: 25 February 2026 | Published online: 14 August 2026

RESEARCH ARTICLE

Journal of Data Science and Intelligent Systems
2026, Vol. 00(00) 1–17
DOI: 10.47852/bonviewJDSIS62027803

BON VIEW PUBLISHING

Ensuring Turmeric Authenticity: A Web-Based AI Approach for Detecting Rice Flour Adulteration

Manhari Palliyaguruge[1], Thilina Abekoon[2], Hirushan Sajindra[3], Rasanjali Samarakoon[1,*], Namal Rathnayake[4] and Upaka Rathnayake[3,*]

[1]*Department of Food Science and Technology, University of Peradeniya, Sri Lanka*

[2]*Water Resources Management and Soft Computing Research Laboratory, Sri Lanka*

[3]*Faculty of Engineering and Design, Atlantic Technological University, Ireland*

[4]*Advanced Institute for Marine Ecosystem Change, Japan Agency for Marine-Earth Science and Technology, Japan*

Abstract: Turmeric powder is widely used for its culinary and medicinal properties. However, its adulteration with substances similar to the properties of pure turmeric powder poses significant concerns regarding quality, authenticity, and consumer health. This study aimed to develop an artificial intelligence (AI)-based tool for detecting rice flour adulteration in turmeric powder using color values and to further validate the findings through chemical, sensory, and microscopic analyses. Pure turmeric powder was mixed with rice flour (0.1%, 0.5%, 1%, 2.5%, 5%, 10%, 15%, 20%, 25%, 30%, 35%, 40%, 45%, 50%, and 100% (w/w)) to create a series of rice flour adulterated turmeric powder samples. The L^*, a^*, and b^* color values were measured and used for the development of the AI tool. Starch iodine complex formation was employed by the iodine test, while sensory evaluation assessed consumer perception to changes in color due to rice flour adulteration in turmeric powder. Microscopic image analysis was utilized to differentiate rice flour adulterated turmeric powder from pure turmeric powder based on the presence of rice flour granules. The results of the iodine test showed its suitability for detecting rice flour adulteration in turmeric powder on a laboratory scale. The AI-based tool enabled rapid and accessible adulteration detection. The findings of this study contribute to enhancing food quality assurance and promoting consumer health by addressing common adulteration practices in turmeric powder.

Keywords: artificial intelligence, rice flour detection, sensory analysis, turmeric adulteration, web-based tool

1. Introduction

Spices and herbs have been valued for centuries for both culinary excellence and medicinal purposes [1]. Beyond enhancing the flavor, aroma, and color of foods, spices are rich in bioactive compounds that contribute to disease prevention and improved health outcomes. Recent scientific interest has highlighted the broad functional spectrum of spices due to constituents such as sulfur compounds, tannins, alkaloids, phenolic diterpenes, flavonoids, and polyphenols [2–5]. Among these, turmeric (*Curcuma longa*) stands out as one of the most recognized and widely used spices across the world owing to its culinary versatility, economic relevance, and substantial bioactive potential [6].

Turmeric, a rhizomatous plant in the Zingiberaceae family, is indigenous to South and Southeast Asia [7] and is cultivated across tropical regions, including Sri Lanka, India, China, Bangladesh, Myanmar, Australia, and the West Indies [8, 9]. Although more than 133 species of Curcuma are identified globally, *Curcuma longa* is most valued because of its industrial and medicinal significance. The rhizome is processed through boiling, drying, and milling to produce the distinctive golden-yellow powder. It is nutritionally rich, containing moisture (84.25%), carbohydrates (9.1%), proteins, lipids, fiber, ash, and essential minerals such as calcium, magnesium, potassium, and sodium [10, 11]. Curcumin, the principal pigment comprising approximately 5.1% of the rhizome, provides potent antioxidant, anti-inflammatory, antimicrobial, and anticancer properties [12, 13].

Beyond its medicinal benefits, turmeric plays an essential role as a functional food ingredient. It stimulates digestive processes by enhancing the activity of pancreatic enzymes, including lipase, amylase, and chymotrypsin [14]. Moreover, when combined with spices such as coriander, cumin, chili, and black pepper, turmeric promotes bile acid secretion, aiding digestion and nutrient metabolism [15]. These properties reinforce the significance of turmeric as both a culinary staple and a nutraceutical ingredient.

Turmeric cultivation is economically important to Sri Lanka, which produced over 25,000 metric tons of raw turmeric in 2020 [16]. Major production districts include Kurunegala, Gampaha, Kalutara, Matale, and Ampara, and approximately 12,900 farmers participate in turmeric cultivation [17]. This crop plays a vital role in rural income generation and small-scale farming systems.

However, the increasing global demand and premium value of turmeric have led to widespread adulteration practices. Economically motivated adulteration involves mixing turmeric powder with cheaper substances such as rice flour, chickpea flour, chalk powder, starch, lead chromate, and metanil yellow [18]. Such adulteration diminishes curcumin concentration, misleads consumers, and may introduce health hazards [19–21]. Although synthetic dyes and toxic heavy metals

*Corresponding author: Rasanjali Samarakoon, Department of Food Science and Technology, University of Peradeniya, Sri Lanka. Email: rasanjalis@agri.pdn.ac.lk and Upaka Rathnayake, Faculty of Engineering and Design, Atlantic Technological University, Ireland. Email: upaka.rathnayake@atu.ie

are known adulterants and extensively studied, comparatively fewer studies address food-based adulterants like rice flour, which closely resemble turmeric in color and composition, making detection more challenging [22, 23]. Conventional analytical approaches, despite their precision, are often time-consuming, labor-intensive, and unsuitable for rapid screening in small-scale processing and commercial settings [24]. There is therefore a growing need for fast, cost-effective, and accurate techniques for spice authentication [25].

In response to this need, the present study explores the application of machine learning integrated with CIELAB colorimetric values for the rapid detection of rice flour adulteration in turmeric powder. The research is guided by the following key questions: (i) Can CIELAB color attributes effectively discriminate between pure and adulterated turmeric samples? (ii) Which machine learning algorithm provides the highest accuracy for predicting adulteration levels? and (iii) Can a user-friendly digital platform be engineered to support real-time adulteration screening?

On the basis of prior evidence that colorimetric characteristics correlate with chemical composition, it is hypothesized that machine learning models trained on CIELAB color data can accurately classify and quantify rice flour adulteration in turmeric powder, whereas the null hypothesis assumes no significant predictive relationship.

To address these questions, this research integrates advanced data analytics and web-based computational tools to design a non-destructive, real-time detection method for turmeric adulteration. This study thus contributes to a scientifically validated, accessible solution for enhancing food quality monitoring and consumer safety within the spice supply chain.

The highlights of this study are as follows:

1) Developed a machine-learning-based web application capable of detecting rice-flour adulteration in turmeric powder with 98% accuracy, utilizing CIELAB color parameters for classification.
2) Employed multi-method validation, including iodine absorbance analysis (R = 0.9866 with rice-flour concentration), sensory evaluation (accurate detection at ≥5% w/w adulteration), and microscopic imaging (marked particle density increase at 20% adulteration), confirming the reliability of adulteration detection.
3) Provides a cost-effective and scalable approach to enhance food safety and consumer protection, with potential for future adaptation to other adulterants and turmeric varieties.

2. Role of Machine Learning in Adulteration Detection

Spices have traditionally been an expensive commodity. Although the general public has access to a variety of spices, safety and quality concerns about spices exist among the community and regulatory authorities. The presence of adulterants that threaten the safety and quality of spices has become a major problem. Some of them are highly toxic to human health. A variety of machine learning (ML) techniques for extracting information from multivariate data have been developed in data science, with recent advances [26].

Artificial intelligence (AI) has become increasingly integrated into the food industry over recent decades, driven by rising global food demand associated with population growth [27–31]. The ability of AI systems to perform tasks such as food quality assessment, process control, food classification, and predictive analysis has significantly increased their adoption within the food sector [32].

In a representative study, Naman et al. [33] developed a machine learning model using transfer learning with MobileNetV2 to identify adulterants in chili pepper (*Capsicum annuum*) with 97.97% accuracy. The approach integrated machine learning with analytical techniques such as HPLC and spectroscopy to ensure robust validation. A similar model using MobileNet achieved 95.5% accuracy in detecting adulterants in cardamom. The study emphasized visual features like color and texture for classification and demonstrated its suitability for real-time, low-power devices [33]. Deep learning models based on CNN and thermal imaging achieved 95.5% accuracy in detecting adulteration in cumin and fennel seeds, proving effective even in distinguishing closely resembling substances [34]. In addition, visible imaging combined with machine learning techniques, including artificial neural networks and support vector machines, has been shown to detect wheat flour adulteration in spice powders such as cinnamon, black pepper, and red pepper with high accuracy [35]. The study by Chen et al. [36] on pericarpium citri reticulatae using machine learning models applied to FT-NIR spectroscopy achieved classification accuracy of up to 99.3% in distinguishing adulterants, outperforming traditional colorimetric methods. CNNs applied to detect adulteration in cinnamon powder achieved over 92% accuracy, while PCA-NIRS methods reached 99.95%, enabling non-specialist access to advanced testing tools [37].

2.1. Starch adulteration in turmeric powder

Many studies have been conducted to develop a machine learning tool using visible-near infrared (Vis-NIR) and multispectral imaging (MSI) techniques to detect starch adulteration in turmeric [18, 38–40]. A set of sample series was prepared by mixing with starch to create spectral and MSI datasets within the 400–1050 nm wavelength range. The findings of these works revealed that Vis-NIR and MSI approaches are excellent in detecting starch adulteration in turmeric with reliability. It has important implications for public health and food safety by offering a reliable tool for verifying the purity of turmeric and other food items [41].

2.2. Rice flour adulteration in turmeric powder

Several studies have been conducted for adulteration in turmeric powder using rice flour and azo dye [42–44]. Bandara et al. [45] conducted multispectral image analysis for detecting the percentage of the common adulterant, tartrazine-colored rice flour, found in Sri Lankan turmeric powder. The sample series was prepared by mixing rice flour with tartrazine (synthetic yellow azo dye, E number E102) at a 9:1 (w/w) ratio. The multispectral imaging system was developed using nine spectral bands with peak wavelengths from 405 nm to 950 nm.

2.3. Sudan dye and metanil yellow adulteration in turmeric powder

Machine learning was used by some researchers to detect the Sudan dye and metanil yellow adulteration in turmeric powder [42, 43, 46]. Mandal et al. [46] used a deep neural network to detect metanil yellow adulteration in turmeric powder. Five variants of pure and adulterated turmeric samples were used in their experiments. They have shown very high accuracy (98%) in detection. In addition, Kar et al. [43] used spectral data of near infrared spectroscopy to detect Sudan dye I adulterant in turmeric powder. They also ended up with high accuracy in detection.

2.4. Research gap in the context of Sri Lankan turmeric

Although there are several machine-learning-based studies on the detection of turmeric adulteration, none of them are based on Sri Lankan turmeric. Bandara et al. [45] showcased some promising results. However, they have not presented a web-based tool in detecting turmeric adulteration percentage. Furthermore, there is a need for a straightforward and simple method to take measurements of adulterated turmeric powder, where the CIELAB method is well suited, as determining the L^*, a^*, and b^* color values are relatively simple and efficient. Therefore, the study presented herein fills the research gap with the novelty of the work carried out.

3. Materials and Methods

3.1. Overall methodology

Figure 1 illustrates the overall workflow of this study, culminating in the development of a web-based analytical tool for predicting the adulteration percentage of turmeric.

3.2. Machine learning models

In this study, neural network (NN), K-nearest neighbors (KNN), decision tree (DT), support vector regression (SVR), and random forest (RF) models were used to predict the adulteration level based on the L^*, a^*, and b^* values of each turmeric sample. The grid search method was employed to identify the best hyperparameters for each model.

3.2.1. Neural network

A neural network is a multi-layered computational model composed of interconnected neurons with weighted connections and non-linear activation functions [47]. Deeper networks with multiple hidden layers can capture hierarchical feature representations [48], enabling them to model highly complex non-linear relationships between inputs and outputs.

In theory, a sufficiently large neural network can approximate almost any continuous function, a concept known as the universal approximation property [49]. In supervised learning, a feedforward process is used, in which the neural network learns to approximate a target function by adjusting its connection weights to minimize the loss between its predictions and the true continuous outputs [50]. Key advantages of NNs include their flexibility and capacity for automatic feature learning from data, which allow them to fit intricate patterns that simpler models might miss [51]. However, they typically require large training datasets and substantial computation to generalize well [52]. NNs are also prone to overfitting if not properly regularized, making interpretation difficult in comparison to simpler models [53].

3.2.2. K-nearest neighbors (KNN)

K-nearest neighbors (KNN) is a non-parametric, instance-based learning algorithm that makes predictions based on the nearest examples in the training data [54]. For regression tasks, the model predicts a numerical outcome by taking the average of the target values of the k most similar training points to the query input [55]. Notably, KNN has no explicit training phase beyond storing the dataset; all generalization is deferred to query time, a characteristic of "lazy" learning methods [54]. This simplicity and the lack of assumptions about data distributions are the advantages of KNNs. They can approximate complex functions given sufficient local data. On the other hand, because it treats all features equally and does not learn feature weights, KNN can be misled by irrelevant or unscaled features [54]. It is also computationally expensive for large datasets, as each prediction requires calculating distances to all training instances, and memory intensive because all data must be kept [56]. Moreover, KNN performs poorly in high-dimensional feature spaces where distance metrics become less informative, thereby degrading their performance [57–59].

3.2.3. Decision tree

A decision tree is a hierarchical model that recursively partitions the feature space into regions, forming a tree of decision nodes and leaves [60]. Each leaf node corresponds to a final prediction. For regression, a tree typically outputs the average of the training target values in a leaf as the predicted value, yielding a piecewise-constant approximation of the underlying function [60]. Decision trees are easy to interpret, and the model can be understood as a set of human-readable "if-then" rules [61]. They can naturally handle non-linear relationships and feature interactions without requiring parametric assumptions. They can also accommodate different types of data and are relatively robust to outliers. However, an unconstrained tree can overfit the training data, as it may keep splitting until each leaf captures very specific cases [62]. Individual decision trees are high-variance estimators where small changes in the training set can drastically change the structure of the learned tree. As a result, decision trees often have moderate predictive accuracy on their own. Techniques like pruning [63] or ensembling [64] are commonly used to improve the generalization performance of decision tree models.

Table 1
Summary of machine learning models for starch adulteration detection in turmeric

Model	Key characteristics	Strengths	Limitations	Performance summary (current study)
Artificial neural network	Multi-layer structure with non-linear activation functions. Learns complex relationships between color values and adulteration level	High accuracy; handles non-linearity and feature interactions well	Requires a large dataset; less interpretable ("black box"); overfitting risk	Moderate performance
Random forest	Ensemble of decision trees using bootstrapped samples and feature randomness	Handles non-linear data well; robust to noise; built-in feature importance metrics	Can be computationally expensive; limited interpretability compared to single trees	Achieved the highest accuracy of 97%; high prediction stability and generalization
Support vector regression	Regression using ε-insensitive loss and kernel functions; focuses on boundary errors	Robust to overfitting; effective for high-dimensional spaces	Sensitive to parameter selection; not easily interpretable	Achieved high accuracy; good performance, less than random forest
Decision tree	Recursive binary splits based on feature thresholds	Easy to interpret; fast training; captures non-linearity	Prone to overfitting; high variance without pruning or ensembling	Moderate performance
K-nearest neighbors	Instance-based, non-parametric; averages outputs from nearest neighbors	Simple; adaptable to data complexity	Computationally intensive at prediction; sensitive to irrelevant features and scaling	Lower performance

Figure 1
Overall methodology

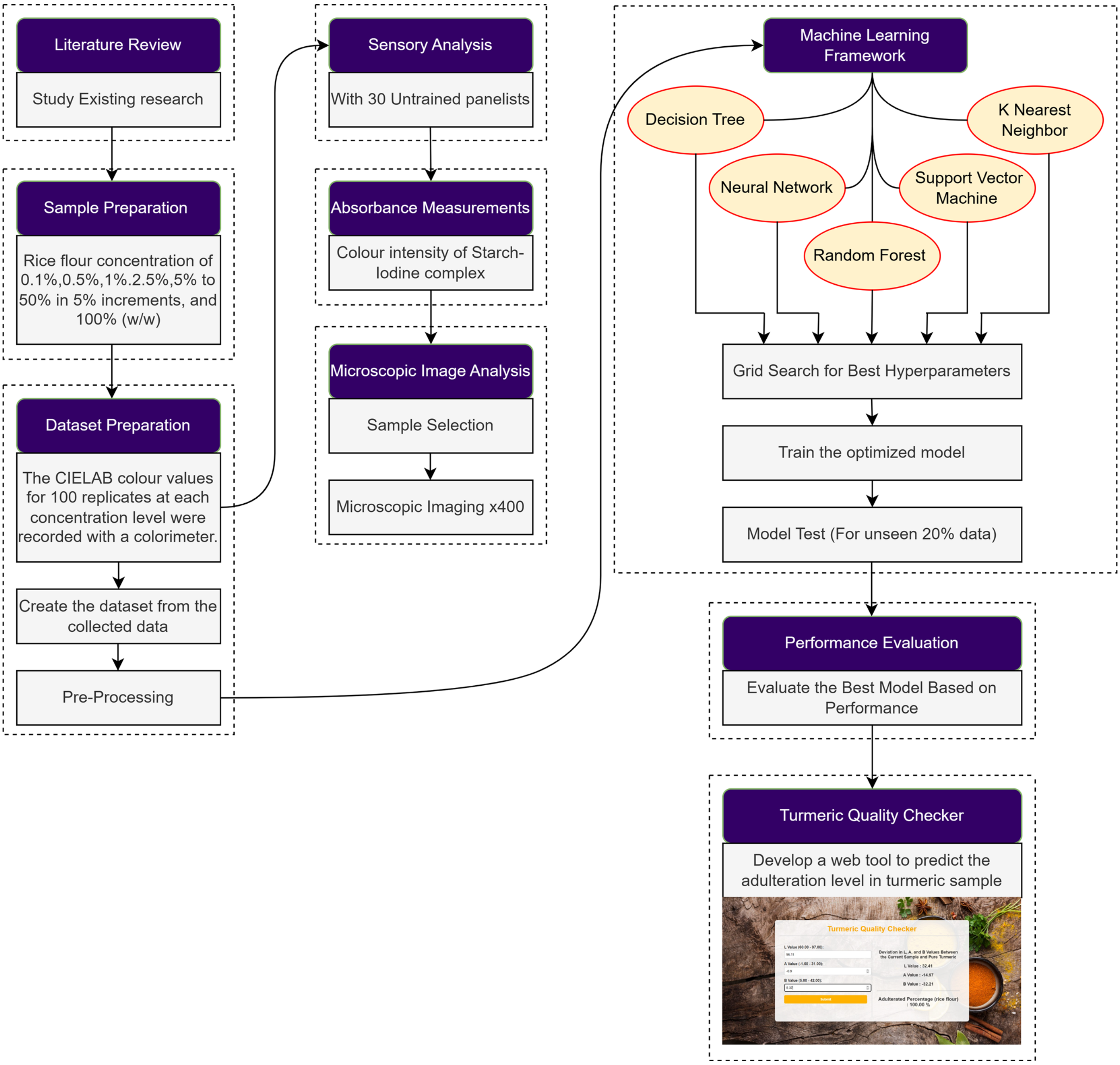

3.2.4. Support vector regression (SVR)

Support vector regression (SVR) was introduced by Vapnik [65] and colleagues in the 1990s as an extension of support vector machines for regression tasks [66]. It operates by fitting a linear prediction function that has at most an € deviation from the true target values for all training points while penalizing deviations larger than €. This is achieved through an € insensitive loss function: errors within ±€ are ignored when fitting the model [67]. The result is a so-called €-tube around the regression function where points inside the tube do not incur loss. Only training samples with errors exceeding € affect the model parameters, leading to a sparse solution that often generalizes well [53]. By using kernel functions, SVR can efficiently handle non-linear regression by implicitly mapping inputs into high-dimensional feature spaces where a linear model can fit complex relationships [68]. SVR is known to be effective in high-dimensional settings and tends to be robust because the margin maximization principle helps in avoiding overfitting. However, training an SVR involves solving a convex quadratic optimization problem, which can be computationally intensive for large datasets [69, 70]. Furthermore, SVR models require careful tuning of hyperparameters, and the resultant models are not very interpretable, as predictions are derived from a combination of support vectors rather than a set of human-readable rules.

3.2.5. Random forest (RF)

Random forest (RF), introduced by Breiman [71], is an ensemble learning method that combines a large number of decision trees to improve predictive performance. Each tree in a random forest is typically trained on a bootstrap-resampled subset of the data (bagging) [72], and at each split, a random subset of features is considered, which injects diversity among the trees [71]. For regression, the prediction of the forest is obtained by averaging the outputs of all individual trees. This aggregation of many de-correlated trees reduces overfitting and yields more stable, accurate predictions than a single tree model [71, 73]. RF inherits many advantages of decision trees—it can handle heterogeneous data types, capture complex non-linear relationships, and is relatively robust to outliers—while mitigating the high-variance weakness of individual trees through averaging. In practice, random forests often achieve high predictive accuracy across a variety of tasks and include an intrinsic measure of feature importance [74–76]. The main limitation is the loss of interpretability. Although each component tree can be interpreted, the ensemble of hundreds of trees is difficult to distill into a simple explanation, which means that random forests trade off the intuitive transparency of single decision trees. In addition, training and using a large number of trees can be computationally demanding, and the model's memory footprint is larger than that of simpler models due to storing many trees. In this study, the random forest model was implemented with 60 trees. The maximum tree depth was set to 80. The model used 70% of the features for each split. The minimum number of samples required to split a node was 5, and the minimum number of samples required at a leaf node was 3. Bootstrap sampling was enabled, and the random state was set to 42 to ensure reproducibility.

Table 1 shows the overall summary of the machine learning models used.

3.3. Adulterated sample preparation

Authentic turmeric powder was prepared using raw turmeric (*Curcuma domestica*) rhizome, which had been planted in February 2024 in Namalthenna Divisional Secretariat, Galagedara, Kandy, Sri Lanka, and harvested in December 2024 (refer to Figure 2).

Raw turmeric rhizomes were washed by dipping in boiling water and then manually sliced into small pieces. Then, the sliced raw turmeric parts were dried in low sunlight for three days and another three days in full sunlight. After that, dried turmeric slices were finely ground and passed through a sieve of 300 µm mesh to obtain powder with a uniform particle size [40]. Turmeric powder and rice flour were mixed for 3 min with a mortar and pestle, rotating 100 anticlockwise and clockwise rotations. These adulteration mixtures were prepared by mixing pure turmeric powder with changing rice flour concentrations of 0.1%, 0.5%, 1%, 2.5%, 5%, 10%, 15%, 20%, 25%, 30%, 35%, 40%, 45%, 50%, and 100% (w/w). One sample was prepared for each concentration, which weighs around 100 g (refer to Figure 3).

3.4. Colorimetric measurements

The colors of the prepared samples were measured using a colorimeter (PCE-CSM, United Kingdom), and the three-color coordinate values were taken as L^*, a^*, and b^*. From each sample, 100 random color readings were taken from pre-determined positions to minimize spatial variation. A non-destructive sampling approach was adopted to replicate realistic market conditions without disturbing the sample packaging. The data obtained were further validated by repeating measurements on a separate day to assess instrument stability.

3.5. Sensory analysis

Sensory analysis was conducted to determine the color variation of the adulterated turmeric powder samples that can be perceived by the human eye. A triangle test was carried out to select the percentages of adulterated turmeric samples that can be perceived by the human eye in terms of color.

Adulterated turmeric percentages 0.1%, 0.5%, 1%, 2.5%, 5%, 10%, 20%, 30%, 40%, and 50% (w/w) were subjected to the study. Thirty untrained panelists from the Faculty of Agriculture, University of Peradeniya, Sri Lanka, were used for the sensory evaluation.

Figure 2
Location of Namalthenna in Sri Lanka

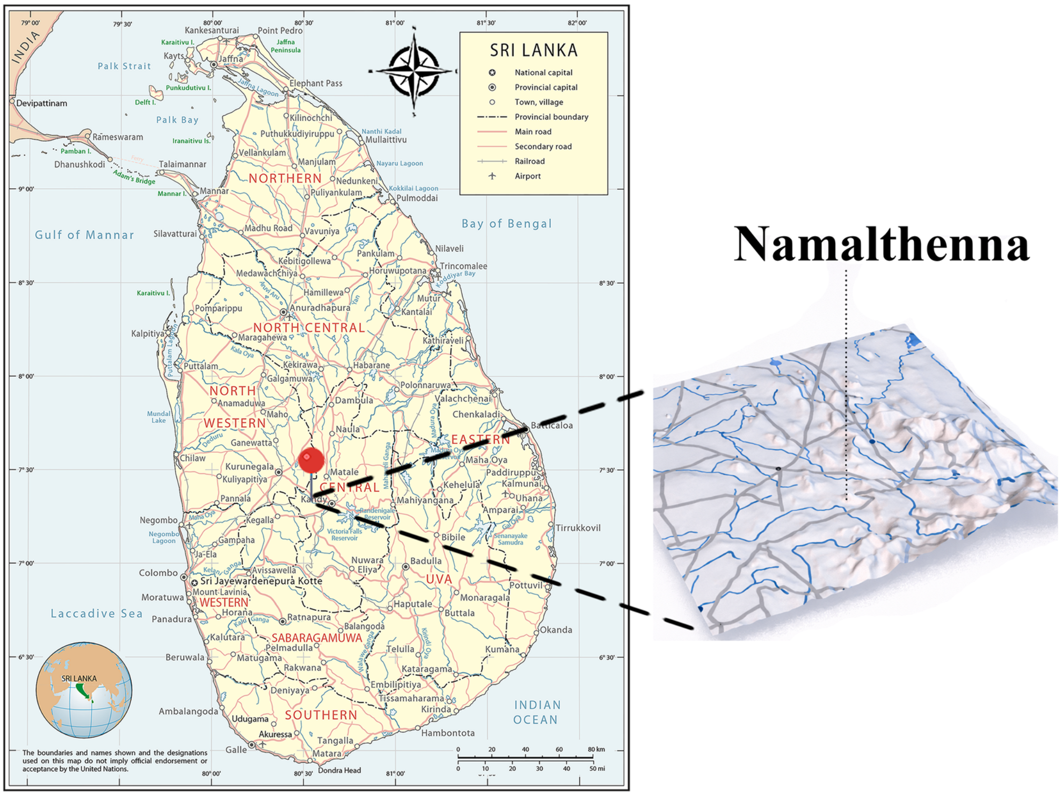

Figure 3
Prepared turmeric samples

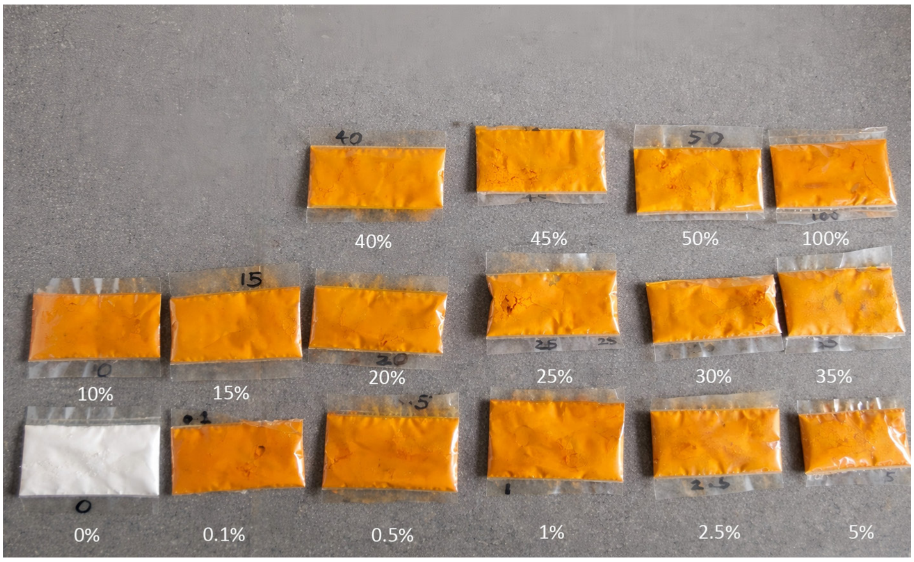

3.6. Absorbance analysis

Each adulterated turmeric sample (100 mg) was mixed with 1 ml of ethanol. Then, 10 ml of 1 N sodium hydroxide was added, and these samples were left overnight. Afterward, the volume was made up to 100 ml. Then, 2.5 ml of the suspension was taken out, and about 20 ml of distilled water was added with three drops of phenolphthalein. Subsequently, a few drops of concentrated hydrochloric acid were added until the pink color disappeared. Then, 1 ml of iodine reagent was added, the volume was brought to 50 ml, and the absorbance was read at 590 nm in UV-Visible spectroscopy (Model: AE-S70-2U, A&E Lab (UK) Co., Ltd.). All chemicals used were of analytical grade, and the experiment was conducted in triplicates.

3.7. Microscopic image analysis

For microscopic analysis, 100 mg of each sample was mixed with 1 ml of distilled water. A 50 µL drop of the suspension was evenly dispersed on a clean glass slide and covered with a coverslip. The prepared slides were examined under a light microscope (Optika, Italy) at 400× magnification, and images were captured to observe the presence and morphology of the rice flour granules in the adulterated turmeric samples.

3.8. Web application development

In this study, five machine learning algorithms were employed, namely, NN, KNN, DT, SVR, and RF. These models were trained on colorimeter readings to predict the percentage of adulteration in turmeric. The dataset was divided into 70% for training, 20% for testing, and 10% for validation. For the non-tree-based algorithms, the color values (L^*, a^*, and b^*) were normalized prior to optimization and training. To facilitate practical use, the best-performing model was integrated into a web-based application.

The AI-powered web application was developed and executed within the Google Colab environment and featured a user-friendly interface [77]. Communication between the client and server was facilitated using an Ngrok tunnel, which functioned as a lightweight API gateway. This configuration provided secure and immediate access over the internet to the locally hosted application, eliminating the need for complex deployment configurations. The primary purpose of the web application is to predict the adulteration level of the turmeric sample by analyzing its L^*, a^*, and b^* color values.

3.9. Statistical analysis

One-way ANOVA was conducted, followed by Tukey's method to determine if the absorbance values differed significantly from one another. Standard deviation, standard error, and confidence interval were calculated to distinguish between the variability of individual data points and the reliability of the estimated population mean.

3.9.1. Standard deviation

Standard deviation quantifies the dispersion or spread of individual measurements around the sample mean (refer to Equation (1)). A higher SD indicates greater variability in the dataset, whereas a lower SD indicates that the measurements are tightly clustered around the mean [78].

$$\text{Standard Deviation} = \sqrt{\frac{\sum (x_i - \bar{x})^2}{n-1}}, \tag{1}$$

Where:
x_i = individual observations
$\bar{x}$ = sample mean
n = number of observations.

3.9.2. Standard error of the mean

The standard error measures how precisely the sample mean estimates the population mean. Unlike standard deviation, the standard error of the mean (refer to Equation (2)) decreases as the number of replicates increases and indicates the reliability of the mean [78].

$$\text{Standard Error of the Mean} = \frac{\text{Standard deviation}}{\sqrt{n}}. \tag{2}$$

3.9.3. Confidence interval (CI)

A 95% confidence interval provides a range in which the true population mean is expected to lie with 95% certainty. CIs express the precision of the mean estimate and are calculated using the standard error and the t-distribution [79] (refer to Equation (3)).

$$\text{Confidence Interval} = \bar{x} \pm t_{\frac{\alpha}{2},df} \times \text{Standard Error of the Mean.} \quad (3)$$

4. Results and Discussion

4.1. Color measurements

Table 2 presents the descriptive statistics of the L^*, a^*, and b^* values to identify the pattern associated with increasing levels of starch adulteration. It includes the mean, standard deviation, standard error of the mean, and the 95% confidence interval of the mean values. In addition, Figure 4 illustrates the histogram distribution of the L^*, a^*, and b^* color parameters at three selected levels of starch adulteration in turmeric powder: low (1%), medium (25%), and high (50%). For each adulteration level, the corresponding distributions show how frequently the observed color values occurred within the sample. At all three adulteration levels, the histograms display an approximately bell-shaped distribution, indicating that the data are close to a normal distribution. The frequency of the measured values tends to cluster around the mean ($\bar{x}$), showing that most samples exhibit similar color intensity within each adulteration category. This pattern reflects low variability and good measurement consistency. Figure 5 shows the deviation of the L^*, a^*, and b^* values with starch adulteration, presented separately. According to the deviations, when starch was added to turmeric powder, the L^* values gradually increased, indicating an increase in lightness. However, the a^* values gradually decreased with adulteration, showing a reduction in the redness of the turmeric. The b^* values remained relatively steady, except at 100% adulteration, where they drastically decreased, indicating a reduction in the yellow color of the turmeric powder.

Table 2
Descriptive statistics with starch adulteration

Sample	Mean (μ)	Standard deviation	Standard error mean	95% confidence interval for μ
L (0%)	63.7040	0.8839	0.0884	(63.5286, 63.8794)
a (0%)	14.066	1.712	0.171	(13.726, 14.406)
b (0%)	37.5749	0.5524	0.0552	(37.4653, 37.6845)
L (0.5%)	64.1756	0.6648	0.0646	(64.0475, 64.3036)
a (0.5%)	12.0380	0.8429	0.0819	(11.8757, 12.2004)
b (0.5%)	39.23	1.0491	0.1024	(39.0276, 39.4324)
L (0.1%)	63.726	2.558	0.251	(63.228, 64.223)
a (0.1%)	12.1122	0.9768	0.0958	(11.9222, 12.3022)
b (0.1%)	38.8086	0.5498	0.0539	(38.7016, 38.9155)
L (1%)	64.1719	0.5578	0.0542	(64.0645, 64.2793)
a (1%)	11.7127	0.5598	0.0544	(11.6049, 11.8206)
b (1%)	40.3986	0.9088	0.0887	(40.2234, 40.5738)
L (2.5%)	65.2095	0.8874	0.0862	(65.0386, 65.3804)
a (2.5%)	12.960	1.651	0.160	(12.642, 13.278)
b (2.5%)	38.8394	0.6977	0.0678	(38.7051, 38.9738)
L (5%)	66.0189	0.7247	0.0711	(65.8780, 66.1599)
a (5%)	14.194	1.401	0.137	(13.922, 14.467)
b (5%)	38.995	2.668	0.262	(38.476, 39.514)
L (10%)	65.925	1.049	0.103	(65.721, 66.129)
a (10%)	12.815	1.628	0.160	(12.498, 13.132)
b (10%)	39.1312	0.8948	0.0877	(38.9572, 39.3053)

Table 2
(*Continued*)

Sample	Mean (μ)	Standard deviation	Standard error mean	95% confidence interval for μ
L (15%)	64.9832	0.6659	0.0666	(64.8511, 65.1153)
a (15%)	11.5658	0.2436	0.0244	(11.5175, 11.6141)
b (15%)	41.741	1.060	0.106	(41.531, 41.952)
L (20%)	65.2774	0.6876	0.0688	(65.1410, 65.4138)
a (20%)	11.3965	0.1682	0.0168	(11.3631, 11.4299)
b (20%)	41.7249	0.9197	0.0920	(41.5424, 41.9074)
L (25%)	66.1028	0.4309	0.0411	(66.0214, 66.1842)
a (25%)	11.2443	0.1159	0.0110	(11.2224, 11.2662)
b (25%)	42.0649	0.7259	0.0692	(41.9277, 42.2021)
L (30%)	66.7078	0.5809	0.0570	(66.5948, 66.8208)
a (30%)	11.0508	0.1410	0.0138	(11.0233, 11.0782)
b (30%)	42.574	2.864	0.281	(42.018, 43.131)
L (35%)	67.1421	0.4418	0.0431	(67.0566, 67.2276)
a (35%)	11.0056	0.4884	0.0477	(10.9111, 11.1001)
b (35%)	42.6856	0.8999	0.0878	(42.5115, 42.8598)
L (40%)	66.2742	0.6294	0.0617	(66.1518, 66.3966)
a (40%)	11.3119	0.2125	0.0207	(11.2708, 11.3530)
b (40%)	42.4886	0.8548	0.0834	(42.3231, 42.6540)
L (45%)	67.893	2.429	0.241	(67.416, 68.370)
a (45%)	10.7377	0.2343	0.0232	(10.6917, 10.7838)
b (45%)	44.349	3.553	0.352	(43.652, 45.047)
L (50%)	69.9270	0.3633	0.0363	(69.8549, 69.9991)
a (50%)	10.1014	0.1480	0.0148	(10.0720, 10.1308)
b (50%)	44.8187	0.7021	0.0702	(44.6794, 44.9580)
L (100%)	95.6564	0.4852	0.0485	(95.5601, 95.7527)
a (100%)	-0.7071	0.2272	0.0227	(-0.7522, -0.6620)
b (100%)	6.655	9.013	0.901	(4.867, 8.444)

Note: *μ:* population mean of color values

4.2. Sensory analysis

Table 3 presents the results of the sensory analysis carried out by 30 untrained panelists. The null hypothesis (H_0) of the study stated that there is no significant difference in color perception between pure turmeric and adulterated samples, while the alternative hypothesis (H_1) stated that there is a significant difference between pure turmeric and turmeric samples adulterated with rice flour. A triangle test was employed to evaluate the responses of 30 untrained panelists.

The critical value at the 0.05 significance level was 15, which means that if 15 or more panelists correctly identified the odd sample, H_0 would be rejected in favor of H_1 by Bolton [80]. Results indicated that color differences between pure and adulterated turmeric samples became statistically perceptible by the sensory panel only at levels of adulteration of 5% (w/w) or higher. At very low levels of adulteration (≤2.5%), including the borderline 1% sample, differences were not accurately detected. Accuracy of detection increased sharply with the increasing level of adulteration to unanimous detection from 10% and upward.

Figure 4
Histograms of L^*, a^*, and b^* color parameters at low, medium, and high levels of starch adulteration in turmeric powder. Subfigures (a), (b), and (c) represent 1% adulteration for L^*, a^*, and b^*, respectively; (d), (e), and (f) represent 25% adulteration for L^*, a^*, and b^*; and (g), (h), and (i) represent 50% adulteration for L^*, a^*, and b^*. The symbol $\bar{x}$ denotes the mean value

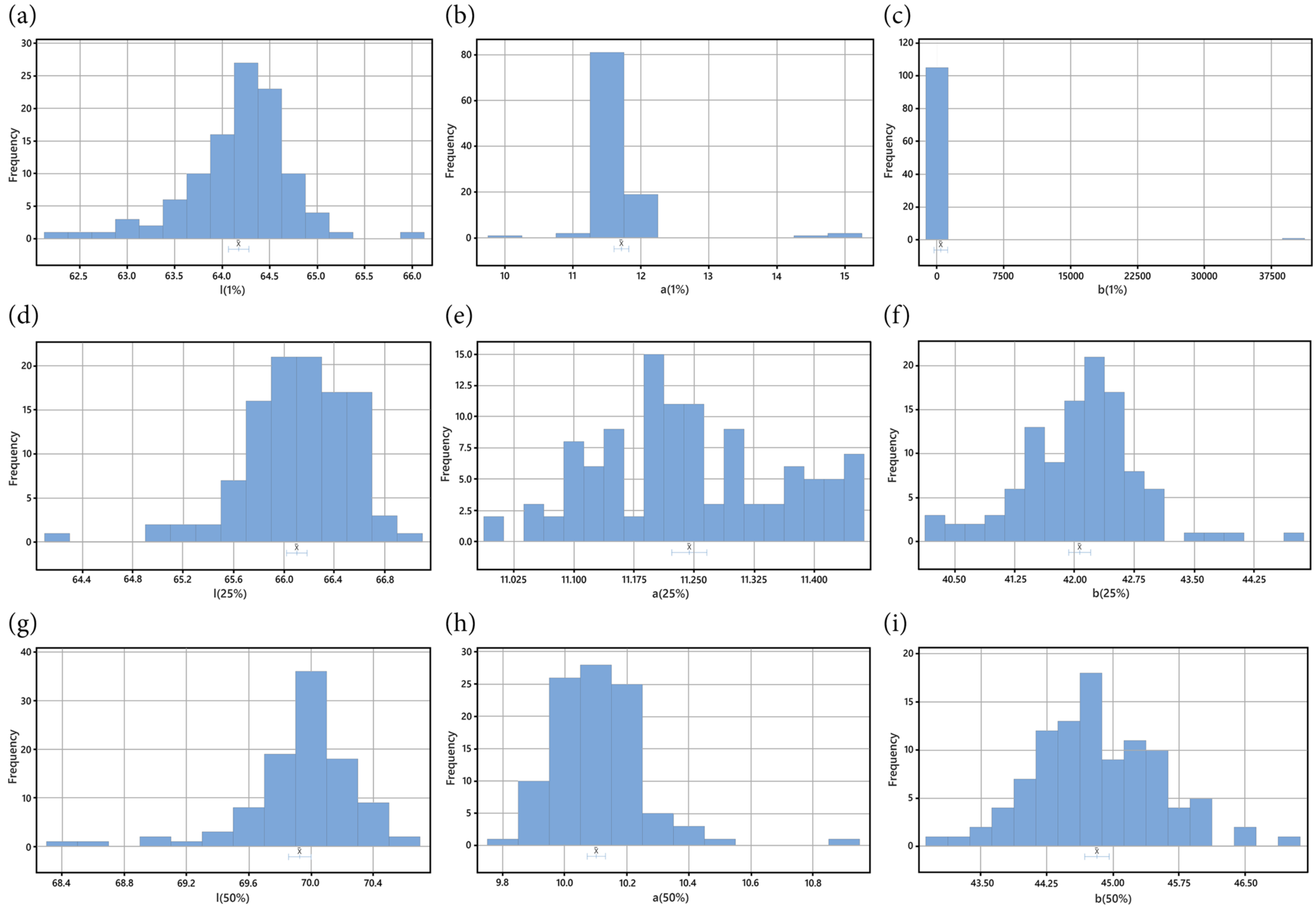

Figure 5
Deviation of color values with percentages of starch adulteration

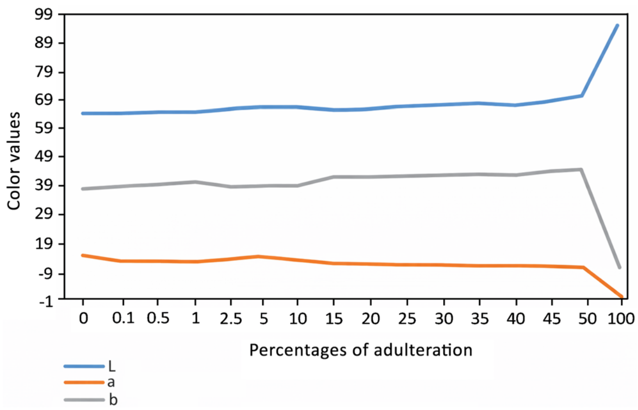

4.3. Absorbance measurements

Starch iodine formation was employed by iodine test. Results of sample series versus absorbance values at 590 nm are listed in Table 4, and the graphical illustration is given in Figure 6. One-way ANOVA method followed by turkey method was conducted to find whether the absorbance values are significantly different from each other. According to the results, there is a significant difference in absorbance values. The 1%–30% and 35%–50% adulteration ranges show relatively steady absorbance, whereas a clear variation is observed when comparing 1%–30%, 35%–50%, and 100% adulteration.

The absorbance values of the adulterated turmeric samples increased with higher proportions of rice flour (refer to Figure 6). At low levels of adulteration (≤20% w/w), the absorbance values remained relatively stable around 0.05–0.07. However, beyond 30% adulteration, a steady increase was observed, reaching a maximum absorbance of 0.255 at 100% rice flour. The regression line indicated a strong positive

Table 3
Results of sensory analysis

Samples assessed	0.1%	0.5%	1%	2.5%	5%	10%	20%	30%	40%	50% (w/w)
Number of correct responses	6	10	14	10	20	29	30	30	30	30

Table 4
Descriptive statistics for absorbance values at 590 nm wavelength

Adulteration percentage (%)	Absorbance values at 590 nm	Standard error mean	95% confidence interval for mean
0	0.020 ± 0.017d	0.010	(-0.0230, 0.0630)
0.1	0.054 ± 0.000c	0.000	(0.05400, 0.05400)
0.5	0.054 ± 0.000c	0.000	(0.05400, 0.05400)
1	0.051 ± 0.004c	0.002	(0.04261, 0.06006)
2.5	0.021 ± 0.001d	0.001	(0.018516,0.023484)
5	0.053 ± 0.004c	0.002	(0.04393, 0.06274)
10	0.0567 ± 0.004c	0.002	(0.04794, 0.06539)
15	0.063 ± 0.022c	0.013	(0.0077, 0.1183)
20	0.065 ± 0.004c	0.002	(0.05506, 0.07494)
25	0.063 ± 0.005c	0.003	(0.05162, 0.07438)
30	0.064 ± 0.003c	0.002	(0.05635, 0.07232)
35	0.099 ± 0.002b	0.001	(0.095539, 0.103128)
40	0.109 ± 0.004b	0.002	(0.10004, 0.11796)
45	0.111 ± 0.002b	0.001	(0.10670, 0.11530)
50	0.121 ± 0.004b	0.002	(0.11204, 0.12996)
100	0.255 ± 0.005a	0.003	(0.24258, 0.26742)

Figure 6
Graphical illustration of absorbance values

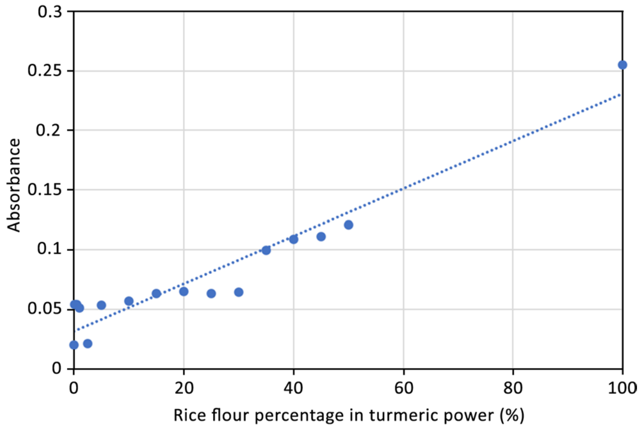

relationship (98.66%) between rice flour concentration and absorbance, suggesting that the iodine test effectively detected adulteration in turmeric powder at higher adulteration (statistically significant %) levels.

Figure 7 presents the results from the one-way ANOVA test. The normal probability plot (refer to Figure 7(a)) for the residuals indicates that the residuals are approximately normally distributed, as the data points closely follow the theoretical straight line. This supports the assumption of normality for the one-way ANOVA. The residuals versus fits plot (refer to Figure 7(b)) shows a random scatter of points around the zero line, with no discernible patterns. This confirms the critical assumption of homoscedasticity among the concentration groups. The histogram of the residuals (refer to Figure 7(c)) is approximately bell-shaped and centered near zero, providing further visual confirmation of the normality assumption. The interval plot (refer to Figure 7(d)) displays the 95% confidence intervals for the mean absorbance value at each level of starch adulteration concentration. The confidence intervals for the lower concentration groups (concentrations 0.1%–30%) largely overlap, suggesting no statistically significant difference in mean absorbance for this range. However, the confidence intervals for the highest concentrations (concentrations 50% and 100%) do not overlap with the lower groups, indicating a statistically significant increase in mean absorbance as starch adulteration increases.

4.4. Microscope image analysis

The prepared sample series were examined under a light microscope. Figure 8 shows the rice flour granules prepared in selected adulterated samples.

Microscopic examination revealed clear visual differences between pure turmeric powder and turmeric adulterated with rice flour. At lower adulteration levels (1%–15%), the field was predominantly occupied by irregularly shaped turmeric particles, which appeared as fine, highly pigmented structures with yellowish to greenish coloration. Only a few semi-transparent, smooth, and more rounded granular characteristics of rice flour were observed scattered within the turmeric matrix, making the identification of adulteration challenging at these low concentrations (Figure 8(a)–(c)).

At higher adulteration levels (20%), the presence of rice flour became visibly distinct, with a marked increase in the number and clustering of these translucent granules (Figure 8(d)). The reduction in pigment density and the increasing proportion of colorless, uniformly shaped particles provided clear microscopic evidence of adulteration. This progressive shift in particle morphology and density with increasing rice flour percentage supports the visual differentiation of pure and adulterated turmeric samples.

4.5. Web application development

On the basis of the performance of the tested machine learning algorithms, the random forest algorithm was selected as the best model. The random forest model utilized the grid search method to identify the optimal parameters. The search included the following: number of trees from 50 to 100 in increments of 10, maximum depth of each tree from 50 to 100 in increments of 10, number of features to consider for the best split from 0.5 to 0.8, and minimum samples required to split a node from 2 to 7. The best parameters selected were n_estimators = 60, max_depth = 80, max_features = 0.7, and min_samples_split = 5. The performance evaluation showed a high coefficient of determination (R^2) of 0.98 for training and 0.97 for testing (refer to Figure 9). In addition, the random forest algorithm showcased the lowest mean squared error. Table 5 presents the performance of each machine learning algorithm.

The relationship between the true and predicted adulteration levels in the validation set is illustrated in Figure 10. The samples were sorted in ascending order of actual adulteration level, and both the actual values (blue) and predicted values (red) are shown, with the dashed black segments indicating the absolute error for each data point. At very low adulteration levels (0–10 data points), the predicted values closely match the actual values. Between approximately 10 and 40 data points, the model shows the largest relative deviations, with several predictions exceeding the true values.

From 100 to 150 data points, the model tends to slightly underestimate the actual values. Overall, the predicted values show noise at the beginning and end of the range, while the mid-range predictions are more stable and closely aligned with the actual data.

The prediction model was used to develop a web-based application, as shown in Figure 11. The web-based application is capable of predicting the adulteration percentage based on the L^*, a^*,

Figure 7
Plots of the one-way ANOVA test. (a) The normal probability plot, (b) residual plot, (c) histogram, and (d) interval plot

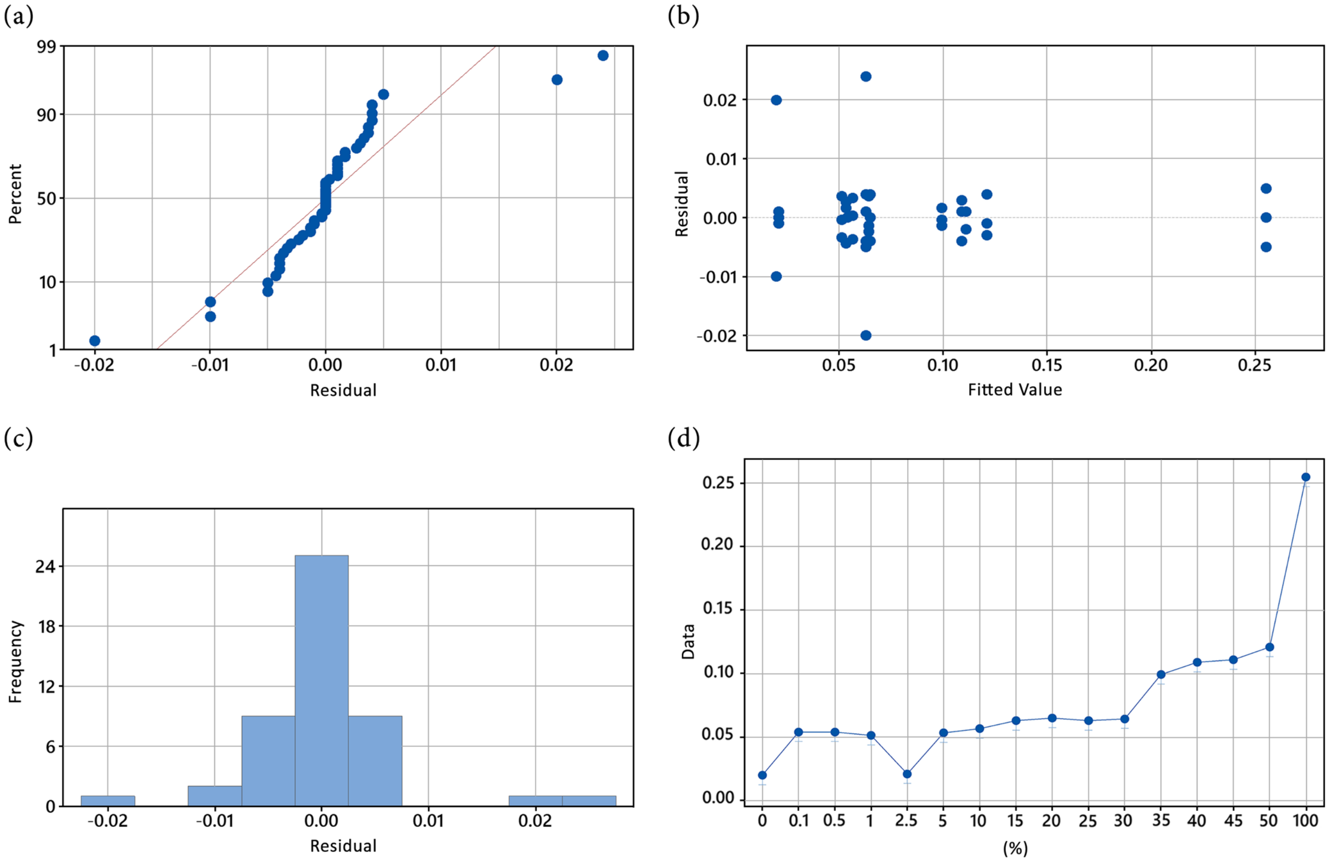

and b^* values of a sample. The web-based application is simple and user-friendly.

The front-end interface was designed using HTML and includes input fields for the L^*, a^*, and b^* color values of a turmeric sample. Users must enter values within a specified range; inputs outside this range trigger an error message. Upon submission of the form, the input data are transmitted to the server via an HTTP POST request. The server, hosted in a cloud environment, runs a pre-trained machine learning algorithm (random forest). This model processes the input to generate a prediction for the adulteration level of the sample.

Once the web application is running, Ngrok initiates a tunneling process on a specified port (port 5000), generating a temporary public URL that points to the local server. This URL is then shared with specific users, allowing them to access the application directly from their browsers via the internet. When a user sends a request through the provided link, Ngrok maps the URL to the corresponding local application and forwards the request through the tunnel to the instance running in the Colab environment. This enables real-time interaction by routing requests from the Ngrok web server to the cloud-hosted application, ensuring a stable and secure data flow.

4.6. Discussion

The integration of multiple analytical methods, including iodine testing, sensory evaluation, and microscopic image analysis, allowed for a holistic approach for identifying and understanding turmeric adulteration. Sensory evaluation, although subjective, added a consumer-level perspective by assessing color. Sensory analysis showed that minor adulteration, such as 0.1%, 0.5%, 1%, and 2.5%, cannot be differentiated from adulterated turmeric powder. Therefore, there is a great need for a comprehensive technique in identifying adulterated turmeric. This will ensure customer protection.

To minimize concentration variability associated with the preparation of multiple samples and to replicate actual market conditions using a non-destructive approach, only one sample package was prepared for each starch adulteration level. However, to ensure representativeness and account for within-sample heterogeneity, color measurements were taken from multiple pre-identified locations on each sample using the colorimeter.

Compared to recent literature, this study aligns closely with the work of Chen et al. [36], who employed FT-NIR spectroscopy alongside a suite of ML algorithms (SVM, KNN, RF, GBM, and PLS-DA) for detecting adulteration in pericarpium citri. Their best models achieved over 99% classification accuracy. However, their reliance on expensive FT-NIR equipment limits broader applicability. In contrast, the present study utilizes cost-effective and accessible methods, including colorimetry and microscopy. Mandal et al. [46] utilized color channel features derived from HSV and YCbCr color spaces, converted from the original RGB space, to detect Sudan I dye adulteration in turmeric powder with high sensitivity. However, their approach targeted synthetic adulterants, whereas the present study focuses on more common starch-based adulteration, which poses a greater visual detection challenge. Naman et al. [33] focused on deep learning (MobileNetV2) to identify adulterated *Capsicum annuum*, achieving 98.67% accuracy using image data and advanced tools like HPLC. In contrast, the presented study herein targeted rice flour adulteration in turmeric powder, a more visually subtle challenge, using interpretable, accessible models based on colorimetric values. Bandara et al. [45]

Figure 8
Microscopic images (40×) of turmeric powder adulterated with rice flour at different levels

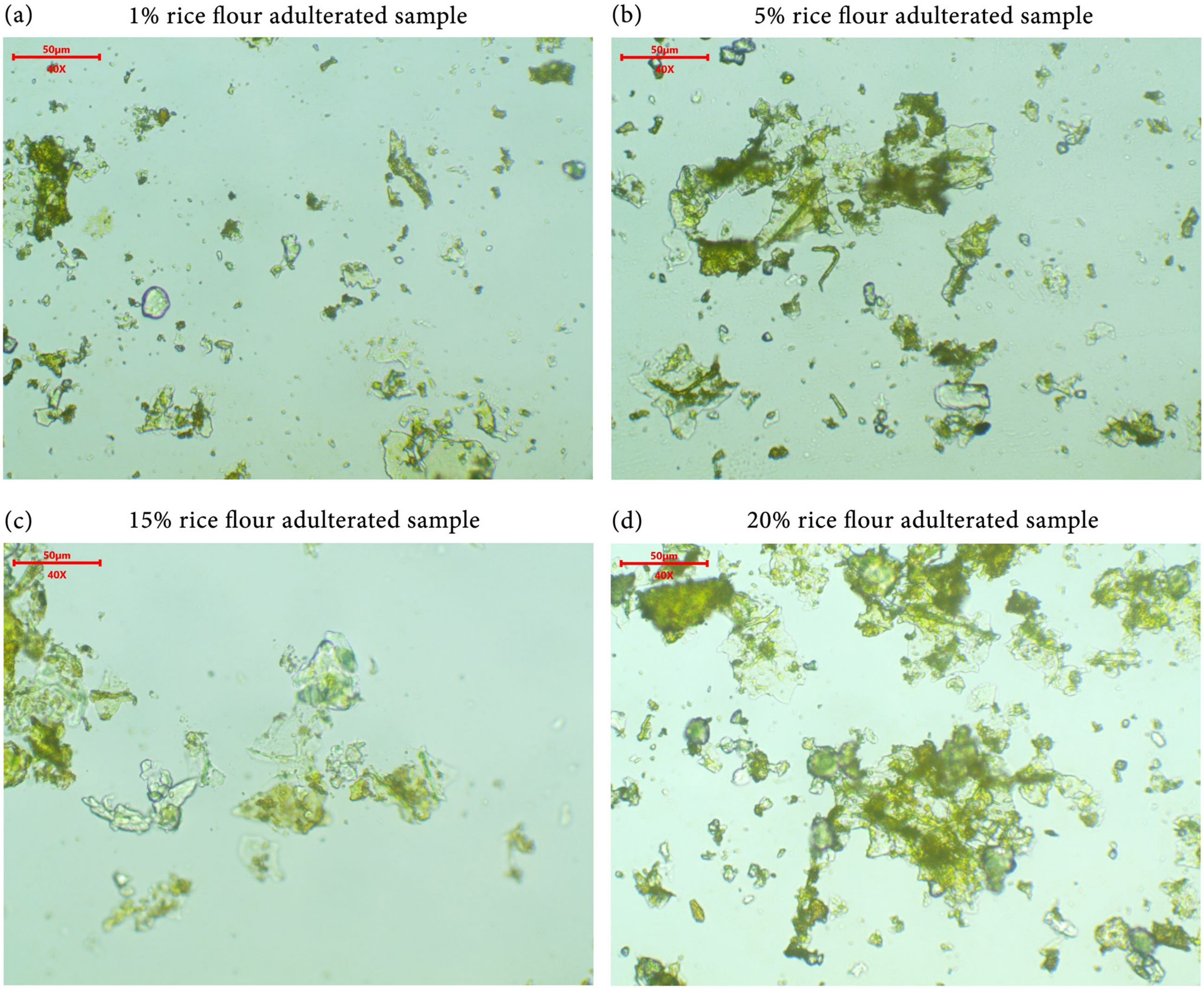

used multispectral imaging with principal component analysis and Bhattacharyya distance to detect turmeric adulteration, achieving high accuracy (R^2 = 0.9911 for modeling; R^2 = 0.9816 for validation) but requiring expensive equipment and laboratory settings. In contrast, the present study developed a low-cost AI-based method using simple color values and validated it with chemical, sensory, and microscopic analyses. This makes the proposed approach more practical, accessible, and suitable for routine quality assurance and real-world applications.

However, the iodine test proved effectively in visually identifying the presence of starch-based adulterants like rice flour, which forms a characteristic blue-black complex with iodine solution. This method can be further developed by increasing sensitivity, removing impurities, or increasing iodine reagent concentration to differentiate even at low levels of rice flour adulteration.

On the other hand, microscopic analysis provided further support, offering visual evidence of adulteration through morphological differences between turmeric and rice flour particles. Microscope image analysis showed that rice flour granules can be seen even in the minute concentration of the rice flour adulterated sample. As a simple laboratory method, microscopy analysis can be carried out to identify rice flour adulteration in pure turmeric. However, this method may not be the best in the perspective of customers as no one is carrying such laboratory instruments to the markets. Nevertheless, iodine and microscopic images can be effectively used by consumer protection authorities.

The development of a web application for detecting rice flour adulteration in turmeric powder represents a significant step toward enhancing food quality and safety. The developed web application has 98% accuracy. However, it would be better if this web-based application could be a mobile app.

4.7. Contribution to Sustainable Development Goals (SDGs)

The research outcome presented here directly deals with Sustainable Development Goals 3 and 12. Consuming adulterated turmeric is a public health issue. Turmeric is not only used as a spice for food, but it is also a health ingredient in most of the Ayurvedic medicine. Therefore, easy identification contributes to food safety and disease prevention. This directly aligns with SDG 3.9—reduce illness from hazardous chemicals and pollution.

In addition, food adulteration undermines sustainable consumption patterns by reducing consumer trust. It is linked with unsustainable supply chains of food production, as it encourages

Figure 9
Comparison of actual and predicted values from the random forest model. Subfigure (a) represents the training set results, while subfigure (b) represents the test set results

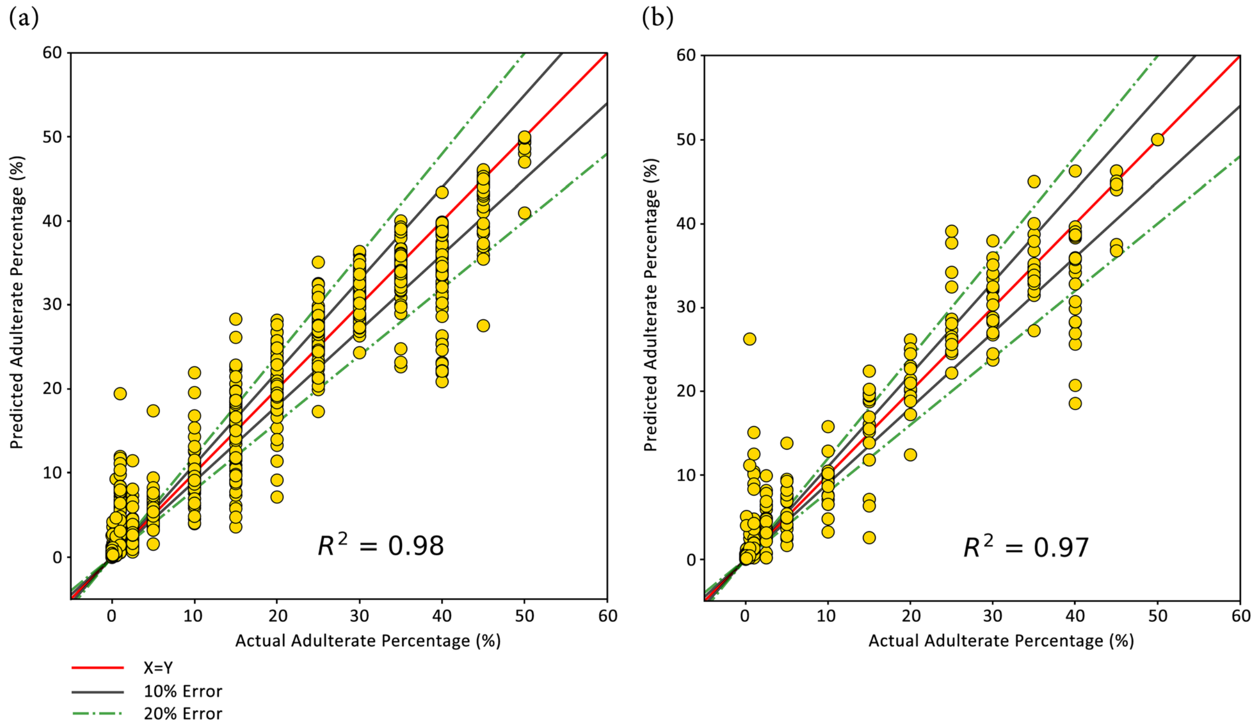

Table 5
Performance of machine learning algorithms

ML algorithm	R^2	Mean squared error	RMSE	NSE	MAE
Neural network	0.9558	33.0315	5.7473	0.9558	4.0797
K-nearest neighbor	0.9582	31.2302	5.5884	0.9582	3.4379
Support vector egression	0.9496	37.6321	6.1345	0.9496	3.6627
Decision tree	0.9660	25.4258	5.0424	0.9660	2.9527
Random forest	0.9742	19.2370	4.3860	0.9742	2.5517

Figure 10
Actual vs. predicted values of the validation set

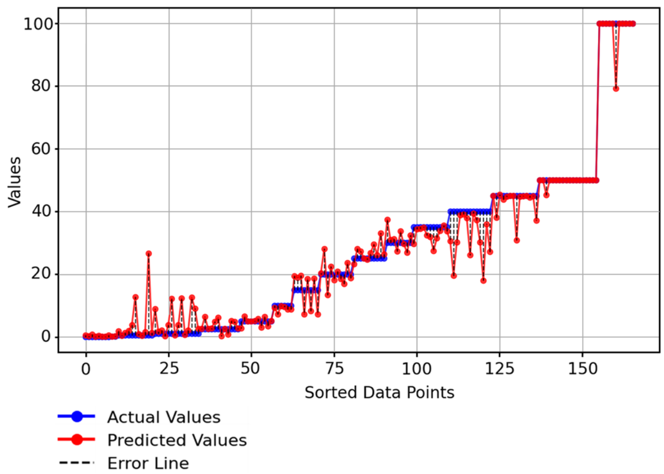

unethical food production. Therefore, the outcome of the work presented herein aligns with SDG 12.3—reduce food loss/waste, 12.6—adopt sustainable practices in companies, and 12.8—promote consumer awareness.

4.8. Limitations and risk of overfitting

The analysis was carried out on a selected turmeric variety grown in the Central Province of Sri Lanka and was only limited to rice flour adulteration. While the random forest model demonstrated strong performance in detecting rice flour adulteration based on colorimetric values, its broader application is subjected to several boundary conditions. Although this model is highly effective for rice flour adulteration, the false-negative and false-positive rates for other potential adulterants, such as corn starch, tapioca starch, or talcum powder, have not been quantified through systematic testing. Therefore, the model should not be applied to detect or exclude the presence of other adulterants. Future work is recommended to involve systematic preparation of replicated samples (≥30 per concentration) at multiple

Figure 11
Interface of web application (L, A, and B represent L^*, a^*, and b^*)

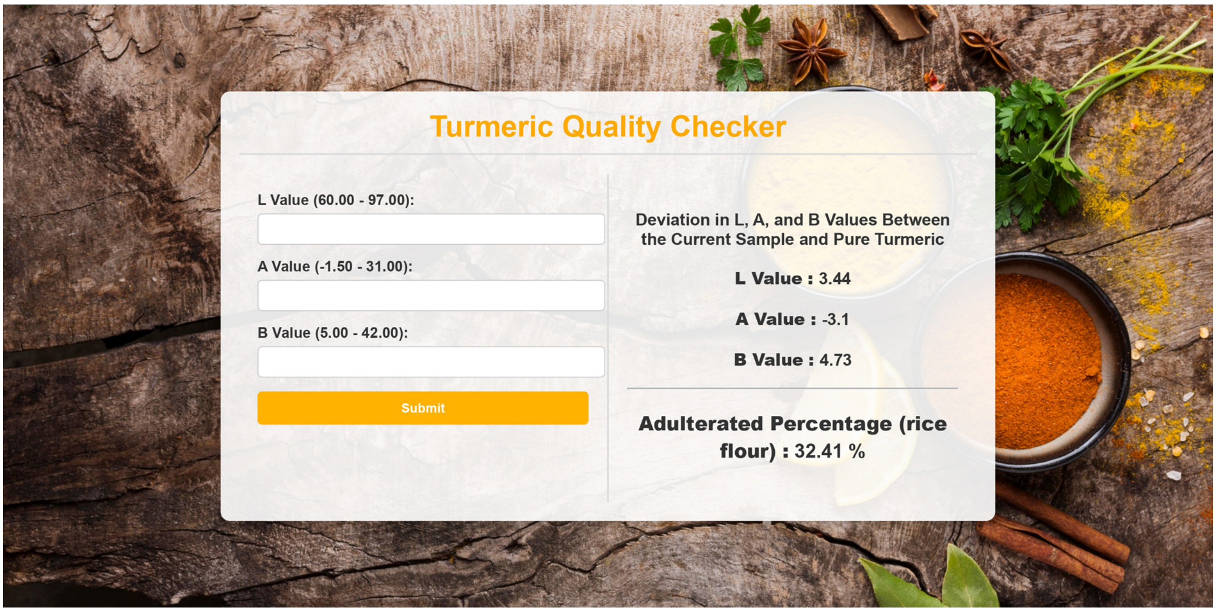

adulteration levels to estimate adulterant-specific classification error rates.

Because each adulterant material has a distinct optical property, their effect on the L^*, a^*, and b^* values could differ accordingly. To validate the robustness of this model, it is recommended that further studies be conducted with prepared samples of turmeric adulterants at varying concentrations of different adulterants.

Similarly, this study has not explored the effect of turmeric's geographical origins or post-harvest treatments on the color measurements.

The color of pure turmeric has vast variability in terms of geographical area, processing methods, preprocessing methods, etc. This study has not assessed the statistical significance of geographic origin (e.g., India, Myanmar, and China) or drying protocol (boiling–sun-drying, hot-air drying, and freeze-drying) on CIELAB values. Because both factors are known to significantly influence turmeric color, their exclusion limits the model's generalizability beyond the specific production conditions investigated.

Recent literature clearly indicates that the CIELAB color parameters (L^*, a^*, and b^*) of turmeric powder are significantly influenced by both geographic origin and post-harvest processing conditions. Turmeric sourced from major producing regions such as India, China, and Myanmar exhibits substantial variability in colorimetric characteristics due to differences in cultivar genetics, agroclimatic conditions, soil mineral composition, and curcuminoid profiles, all of which directly affect optical properties and perceived color [38, 42]. In addition to origin-related effects, drying protocols play a statistically significant role in determining turmeric color, as thermal exposure and moisture removal kinetics influence pigment stability, surface scattering, and oxidative degradation. Studies by Lanjewar et al. [18] and Johnson et al. [25] employing spectroscopic and imaging techniques have shown that traditional sun-drying and hot-air drying often result in increased lightness (L^*) and reduced chromatic intensity (a^* and b^*), whereas controlled drying methods better preserve yellowness and color saturation. Although these studies collectively demonstrate that both geographic origin and drying method can introduce statistically significant shifts in CIELAB values, the present study intentionally controlled for these variables using turmeric from a single Sri Lankan region processed exclusively by boiling followed by sun-drying. This design minimized confounding variability and enabled focused evaluation of rice flour adulteration effects, while statistical assessment of origin- and processing-induced color variation was beyond the scope of this work and remains an important direction for future model generalization.

It is therefore highly recommended to repeat the work in other geographic areas where turmeric is grown, at least in Sri Lanka, and with different processing conditions. Given these limitations, **this model should currently be applied to turmeric grown in the Central Province of Sri Lanka**, which has been processed using the boiling and sun-drying method, and adulterated with rice flour only. Therefore, to ensure broader applicability and minimize the risk of overfitting, future studies should include more diverse turmeric sources, processing conditions, and adulterants.

5. Conclusions

This study successfully developed a web-based application capable of detecting rice flour adulteration in turmeric powder by measuring the colorimetric values in addition to the integration of other detection methods: starch-iodine complex formation testing, sensory evaluation, and microscopic image analysis. Each method contributed uniquely to the identification of adulteration, offering a multi-faceted approach that balances technical accuracy with user accessibility. The iodine test indicated the increment in absorbance values and microscopic analysis provided reliable visual indicators of adulteration, while sensory analysis offered insight into how consumers might perceive the color of the adulterated turmeric.

The machine-learning-enabled web-based tool is reliable with high predictive accuracy in predicting turmeric adulteration percentage. While currently limited to a specific turmeric variety and rice flour adulteration, the approach provides a foundation for scalable, cost-effective, and accessible adulteration detection methods. The developed model should currently be applied only to turmeric produced in the Central Province of Sri Lanka, processed using traditional boiling-and-sun-drying methods, and adulterated exclusively with rice flour. Future improvements can be focused on extending the model to different turmeric varieties, incorporating multiple adulterants, and developing mobile applications for practical use by regulators and consumers.

Ethical Statement

This study does not contain any studies with human or animal subjects performed by any of the authors.

Conflicts of Interest

The authors declare that they have no conflicts of interest to this work.

Data Availability Statement

Data are available from the corresponding author upon reasonable request.

Author Contribution Statement

Manhari Palliyaguruge: Methodology, Formal analysis, Investigation, Resources, Data curation, Writing – original draft, Visualization. **Thilina Abekoon:** Formal analysis, Data curation, Writing – review & editing. **Hirushan Sajindra:** Software, Formal analysis, Data curation, Writing – review & editing. **Rasanjali Samarakoon:** Conceptualization, Validation, Supervision, Project administration. **Namal Rathnayake:** Validation, Data curation. **Upaka Rathnayake:** Conceptualization, Validation, Writing – review & editing, Supervision, Project administration.

References

[1] Łuczaj, Ł., Dumanowski, J., Marszałek, C., & Parasecoli, F. (2023). Turmeric and cumin instead of stock cubes: An internet survey of spices and culinary herbs used in Poland compared with historical cookbooks and herbals. *Plants*, *12*(3), 591. https://doi.org/10.3390/plants12030591

[2] Charneca, S., Hernando, A., Costa-Reis, P., & Guerreiro, C. S. (2023). Beyond seasoning—The role of herbs and spices in rheumatic diseases. *Nutrients*, *15*(12), 2812. https://doi.org/10.3390/nu15122812

[3] Dahl, S. M., Rolfe, V., Walton, G. E., & Gibson, G. R. (2023). Gut microbial modulation by culinary herbs and spices. *Food Chemistry*, *409*, 135286. https://doi.org/10.1016/j.foodchem.2022.135286

[4] Herrera, T., Iriondo-DeHond, A., Uribarri, J., & del Castillo, M. D. (2025). Beneficial herbs and spices. In J. Uribarri & J. A. Vassalotti (Eds.), *Nutrition, fitness, and mindfulness: An evidence-based guide for clinicians* (2nd ed., pp. 115–137). Springer. https://doi.org/10.1007/978-3-031-87441-3_9

[5] Mackonochie, M., Rodriguez-Mateos, A., Mills, S., & Rolfe, V. (2023). A scoping review of the clinical evidence for the health benefits of culinary doses of herbs and spices for the prevention and treatment of metabolic syndrome. *Nutrients*, *15*(23), 4867. https://doi.org/10.3390/nu15234867

[6] Lanjewar, M. G., Morajkar, P. P., & Parab, J. (2022). Detection of tartrazine colored rice flour adulteration in turmeric from multi-spectral images on smartphone using convolutional neural network deployed on PaaS cloud. *Multimedia Tools and Applications*, *81*(12), 16537–16562. https://doi.org/10.1007/s11042-022-12392-3

[7] Govindarajan, V. S., & Stahl, W. H. (1980). Turmeric—Chemistry, technology, and quality. *C R C Critical Reviews in Food Science and Nutrition*, *12*(3), 199–301. https://doi.org/10.1080/10408398009527278

[8] Fuloria, S., Mehta, J., Chandel, A., Sekar, M., Rani, N. N. I. M., Begum, M. Y., …, & Fuloria, N. K. (2022). A comprehensive review on the therapeutic potential of *Curcuma longa* Linn. in relation to its major active constituent curcumin. *Frontiers in Pharmacology*, *13*, 820806. https://doi.org/10.3389/fphar.2022.820806

[9] Saensouk, P., Saensouk, S., Chanthavongsa, K., Sengthong, A., Phengmala, K., Maknoi, C., …, & Boonma, T. (2025). Seven new records of *Curcuma* L. (Zingiberaceae) for the flora of Laos: Implications for biodiversity conservation and sustainable horticulture. *Horticulturae*, *11*(7), 720. https://doi.org/10.3390/horticulturae11070720

[10] Ayodeji, A., & Liu, Y.-K. (2018). SVR optimization with soft computing algorithms for incipient SGTR diagnosis. *Annals of Nuclear Energy*, *121*, 89–100. https://doi.org/10.1016/j.anucene.2018.07.011

[11] Mane, R. P., Kshirsagar, R. B., Sawate, A. R., Patil, B. M., & Kale, R. G. (2018). Studies on evaluation of physicochemical and nutritional properties of fresh turmeric rhizome. *Journal of Pharmacognosy and Phytochemistry*, *7*(2), 2895–2897.

[12] Cozmin, M., Lungu, I. I., Gutu, C., Stefanache, A., Duceac, L. D., Șoltuzu, B. D., …, & Boev, M. (2024). Turmeric: From spice to cure. A review of the anti-cancer, radioprotective and anti-inflammatory effects of turmeric sourced compounds. *Frontiers in Nutrition*, *11*, 1399888. https://doi.org/10.3389/fnut.2024.1399888

[13] El-Saadony, M. T., Saad, A. M., Mohammed, D. M., Alkafaas, S. S., Ghosh, S., Negm, S. H., …, & El-Tarabily, K. A. (2025). Curcumin, an active component of turmeric: Biological activities, nutritional aspects, immunological, bioavailability, and human health benefits—A comprehensive review. *Frontiers in Immunology*, *16*, 1603018. https://doi.org/10.3389/fimmu.2025.1603018

[14] Alhar, M. S. O., El-Sofany, W. I., AlRashidi, A. A., & Hamden, K. (2025). Protective effects of isolated curcumin from *Curcuma longa* on key enzymes involved in the insulin signaling pathway and digestive and metabolic enzymes associated with obesity, type 2 diabetes, and hypertension. *Journal of Diabetes Research*, *2025*(1), 8050374. https://doi.org/10.1155/jdr/8050374

[15] Irshad, A., Rasane, P., Gurumayum, S., Singh, J., Kaur, S., Patel, A. S., …, & Sharma, K. (2024). Interaction of human gut microflora with commonly consumed herbs and spices: A review. *Current Nutrition & Food Science*, *20*(3), 317–330. https://doi.org/10.2174/1573401319666230412110343

[16] Vidanapathirana, N. P., Subasinghe, S., Sunil, K., Ketipearachchi, K. G., Siriwardana, A. J. M. C. M., & Bandusekara, B. S. (2022). Growth and yield performances of turmeric (*Curcuma longa*) grown in dry zone of Sri Lanka as affected by planting space, growing media and shade. *Journal of Agro-Technology and Rural Sciences*, *1*(2), 27–31. https://doi.org/10.4038/atrsj.v1i2.32

[17] Abeynayaka, A. A. S. L., Bandara, A. M. K. R., Lankapura, A. I. Y., & Idamekorala, P. R. (2020). Economics of turmeric production in Sri Lanka: An empirical analysis in major turmeric growing districts. *Asian Journal of Agricultural and Horticultural Research*, *6*(4), 10–17. https://doi.org/10.9734/ajahr/2020/v6i430078

[18] Lanjewar, M. G., Asolkar, S., Parab, J. S., & Morajkar, P. P. (2024). Detecting starch-adulterated turmeric using Vis-NIR spectroscopy and multispectral imaging with machine learning. *Journal of Food Composition and Analysis*, *136*, 106700. https://doi.org/10.1016/j.jfca.2024.106700

[19] Dixit, S., Purshottam, S. K., Khanna, S. K., & Das, M. (2009). Surveillance of the quality of turmeric powders from city markets of India on the basis of curcumin content and the presence of extraneous colours. *Food Additives & Contaminants: Part A*, *26*(9), 1227–1231. https://doi.org/10.1080/02652030903016586

[20] Thangaraju, S., Modupalli, N., & Natarajan, V. (2021). Food adulteration and its impacts on our health/balanced nutrition. In M. Sen (Ed.), *Food chemistry: The role of additives, preservatives and adulteration* (pp. 189–216). Wiley. https://doi.org/10.1002/9781119792130.ch7

[21] Momtaz, M., Bubli, S. Y., & Khan, M. S. (2023). Mechanisms and health aspects of food adulteration: A comprehensive review. *Foods*, *12*(1), 199. https://doi.org/10.3390/foods12010199

[22] Velázquez, R., Rodríguez, A., Hernández, A., Casquete, R., Benito, M. J., & Martín, A. (2023). Spice and herb frauds: Types, incidence, and detection: The state of the art. *Foods*, *12*(18), 3373. https://doi.org/10.3390/foods12183373

[23] You, H., Gershon, H., Goren, F., Xue, F., Kantowski, T., & Monheit, L. (2022). Analytical strategies to determine the labelling accuracy and economically-motivated adulteration of "natural" dietary supplements in the marketplace: Turmeric case study. *Food Chemistry*, *370*, 131007. https://doi.org/10.1016/j.foodchem.2021.131007

[24] Prabhath, G. W. K., Bandara, W. G. C., Dissanayake, D. W. S. C. B., Hearath, H. M. V. R., Godaliyadda, G. M. R. I., Ekanayake, M. P. B., …, & Madhujith, T. (2019). Multispectral imaging for detection of adulterants in turmeric powder. In *Optical Sensors and Sensing Congress*, HTu3B.3. https://doi.org/10.1364/HISE.2019.HTu3B.3

[25] Johnson, N. A. N., Adade, S. Y.-S. S., Ekumah, J.-N., Kwadzokpui, B. A., Xu, J., Xu, Y., & Chen, Q. (2025). A comprehensive review of analytical techniques for spice quality and safety assessment in the modern food industry. *Critical Reviews in Food Science and Nutrition*, *65*(30), 7225–7250. https://doi.org/10.1080/10408398.2025.2462721

[26] Sajindra, H., Dharmawansha, S., Wijesundara, H., Herath, S., Rathnayake, U., & Meddage, D. (2025). Hybrid neural network methods to model the external wind pressure on a low-rise flat-roofed building in an irregularly shaped urban environment. *Structures*, *79*, 109529. https://doi.org/10.1016/j.istruc.2025.109529

[27] Addanki, M., Patra, P., & Kandra, P. (2022). Recent advances and applications of artificial intelligence and related technologies in the food industry. *Applied Food Research*, *2*(2), 100126. https://doi.org/10.1016/j.afres.2022.100126

[28] Ben Ayed, R., & Hanana, M. (2021). Artificial intelligence to improve the food and agriculture sector. *Journal of Food Quality*, *2021*(1), 5584754. https://doi.org/10.1155/2021/5584754

[29] Bidyalakshmi, T., Jyoti, B., Mansuri, S. M., Srivastava, A., Mohapatra, D., Kalnar, Y. B., …, & Indore, N. (2025). Application of artificial intelligence in food processing: Current status and future prospects. *Food Engineering Reviews*, *17*(1), 27–54. https://doi.org/10.1007/s12393-024-09386-2

[30] Ding, H., Tian, J., Yu, W., Wilson, D. I., Young, B. R., Cui, X., …, & Li, W. (2023). The application of artificial intelligence and big data in the food industry. *Foods*, *12*(24), 4511. https://doi.org/10.3390/foods12244511

[31] Sharma, S., Gahlawat, V. K., Rahul, K., Mor, R. S., & Malik, M. (2021). Sustainable innovations in the food industry through artificial intelligence and big data analytics. *Logistics*, *5*(4), 66. https://doi.org/10.3390/logistics5040066

[32] Goyal, R., Singha, P., & Singh, S. K. (2025). Machine learning-assisted Fourier transform infrared spectroscopy to predict adulteration in coriander powder. *Food Chemistry*, *477*, 143502. https://doi.org/10.1016/j.foodchem.2025.143502

[33] Naman, S., Sharma, S., & Baldi, A. (2024). Identification of spices and their adulterants by integrating machine learning and analytical techniques: A representative study. *International Journal of Pharmaceutical Sciences and Drug Research*, *16*(3), 359–369. https://doi.org/10.25004/ijpsdr.2024.160307

[34] Hajera, M., Santhi, M., & Divya, B. (2023). Detection of cumin seeds adulteration based on thermal imaging using deep learning technique. *International Journal of Scientific Research in Engineering and Management*, *07*(10), 1–7. https://doi.org/10.55041/ijsrem25972

[35] Kheiralipour, K., & Nargesi, M. H. (2024). Classification of wheat flour levels in powdered spices using visual imaging. *Journal of Agriculture and Food Research*, *18*, 101408. https://doi.org/10.1016/j.jafr.2024.101408

[36] Chen, Y., Li, S., Jia, J., Sun, C., Cui, E., Xu, Y., …, & Tang, A. (2024). FT-NIR combined with machine learning was used to rapidly detect the adulteration of pericarpium citri reticulatae (*chenpi*) and predict the adulteration concentration. *Food Chemistry: X*, *24*, 101798. https://doi.org/10.1016/j.fochx.2024.101798

[37] Ku, H.-H., Liao, Y.-C., & Chi, C.-H. (2023). Deep learning applied on cinnamon powder adulteration detection. In *2023 IEEE 6th International Conference on Knowledge Innovation and Invention*, 324–327. https://doi.org/10.1109/ICKII58656.2023.10332797

[38] Amsaraj, R., Ranjan, R., Rachaiah, B. P., & Mutturi, S. (2024). Multi-instrument spectroscopic study for authentication of curcumin content in commercial turmeric powders using machine learning algorithms. *Journal of Food Composition and Analysis*, *134*, 106543. https://doi.org/10.1016/j.jfca.2024.106543

[39] Lanjewar, M. G., Asolkar, S. S., & Parab, J. S. (2024). Hybrid methods for detection of starch in adulterated turmeric from colour images. *Multimedia Tools and Applications*, *83*(25), 65789–65814. https://doi.org/10.1007/s11042-024-18195-y

[40] Lanjewar, M. G., Morajkar, P. P., & Parab, J. S. (2024). Portable system to detect starch adulteration in turmeric using NIR spectroscopy. *Food Control*, *155*, 110095. https://doi.org/10.1016/j.foodcont.2023.110095

[41] Sahoo, A., Kar, B., Sahoo, S., Jena, S., Kuanar, A., Parameswaran, S., …, & Nayak, S. (2019). *De Novo* transcriptome sequencing explored cultivar specific sequence variation and differential expression of pigment synthesis genes in turmeric (*Curcuma longa* L.). *Industrial Crops and Products*, *134*, 388–402. https://doi.org/10.1016/j.indcrop.2019.04.021

[42] Abia, W. A., Haughey, S. A., Radhika, R., Taty, B. P., Russell, H., Carey, M., …, & Williams, P. N. (2025). Africa, an emerging exporter of turmeric: Combating fraud with rapid detection systems. *Foods*, *14*(9), 1590. https://doi.org/10.3390/foods14091590

[43] Kar, S., Tudu, B., & Bandyopadhyay, R. (2024). Statistical machine learning techniques applied to NIR spectral data for rapid detection of Sudan dye-I in turmeric powders with optimized pre-processing and wavelength selection. *Journal of Food Science and Technology*, *61*(10), 1955–1964. https://doi.org/10.1007/s13197-024-05971-9

[44] Mandal, D., Chatterjee, A., & Tudu, B. (2022). A color channel based on multiple random forest coupled with a computer

vision technique for the detection and prediction of Sudan dye-I adulteration in turmeric powder. *Color Research & Application*, *47*(2), 388–400. https://doi.org/10.1002/col.22741

[45] Bandara, W. G. C., Kasun Prabhath, G. W., Sahan Chinthana Bandara Dissanayake, D. W., Herath, V. R., Roshan Indika Godaliyadda, G. M., Bandara Ekanayake, M. P., …, & Madhujith, T. (2020). Validation of multispectral imaging for the detection of selected adulterants in turmeric samples. *Journal of Food Engineering*, *266*, 109700. https://doi.org/10.1016/j.jfoodeng.2019.109700

[46] Mandal, D., Chatterjee, A., & Tudu, B. (2022). A deep neural network and random forests driven computer vision framework for identification and prediction of metanil yellow adulteration in turmeric powder. *Concurrency and Computation: Practice and Experience*, *34*(1), e6500. https://doi.org/10.1002/cpe.6500

[47] Dey, P. (2025). *Computational cytology: Advancements and applications with artificial intelligence*. Singapore: Springer. https://doi.org/10.1007/978-981-95-3272-8

[48] Islam, M. T., & Lei, X. (2024). Deciphering the feature representation of deep neural networks for high-performance AI. *IEEE Transactions on Pattern Analysis and Machine Intelligence*, *46*(8), 5273–5287. https://doi.org/10.1109/tpami.2024.3363642

[49] Geuchen, P., Jahn, T., & Matt, H. (2025). Universal approximation with complex-valued deep narrow neural networks. *Constructive Approximation*, *62*(2), 361–402. https://doi.org/10.1007/s00365-025-09713-8

[50] Mallikarjunaiah, S. M. (2023). A deep learning feed-forward neural network framework for the solutions to singularly perturbed delay differential equations. *Applied Soft Computing*, *148*, 110863. https://doi.org/10.1016/j.asoc.2023.110863

[51] Tian, C., Cheng, T., Peng, Z., Zuo, W., Tian, Y., Zhang, Q., …, & Zhang, D. (2025). A survey on deep learning fundamentals. *Artificial Intelligence Review*, *58*(12), 381. https://doi.org/10.1007/s10462-025-11368-7

[52] Ahmed, S. F., Alam, M. S. B., Hassan, M., Rozbu, M. R., Ishtiak, T., Rafa, N., …, & Gandomi, A. H. (2023). Deep learning modelling techniques: Current progress, applications, advantages, and challenges. *Artificial Intelligence Review*, *56*(11), 13521–13617. https://doi.org/10.1007/s10462-023-10466-8

[53] Zhang, B., He, Z., & Lin, H. (2024). A comprehensive review of deep neural network interpretation using topological data analysis. *Neurocomputing*, *609*, 128513. https://doi.org/10.1016/j.neucom.2024.128513

[54] Halder, R. K., Uddin, M. N., Uddin, M. A., Aryal, S., & Khraisat, A. (2024). Enhancing K-nearest neighbor algorithm: A comprehensive review and performance analysis of modifications. *Journal of Big Data*, *11*(1), 113. https://doi.org/10.1186/s40537-024-00973-y

[55] Loeloe, M. S., Tabatabaei, S. M., Sefidkar, R., Mehrparvar, A. H., & Jambarsang, S. (2025). Boosting K-nearest neighbor regression performance for longitudinal data through a novel learning approach. *BMC Bioinformatics*, *26*(1), 232. https://doi.org/10.1186/s12859-025-06205-1

[56] Rajabinasab, M., Pakdaman, F., Zimek, A., & Gabbouj, M. (2025). Randomized PCA forest for approximate k-nearest neighbor search. *Expert Systems with Applications*, *281*, 126254. https://doi.org/10.1016/j.eswa.2024.126254

[57] Lu, J., & Gweon, H. (2025). Random k conditional nearest neighbor for high-dimensional data. *PeerJ Computer Science*, *11*, e2497. https://doi.org/10.7717/peerj-cs.2497

[58] Ting, K. M., Washio, T., Zhu, Y., Xu, Y., & Zhang, K. (2024). Is it possible to find the single nearest neighbor of a query in high dimensions? *Artificial Intelligence*, *336*, 104206. https://doi.org/10.1016/j.artint.2024.104206

[59] Liu, Y., Zhang, Y., Wang, X., & Qu, X. (2025). Evidential K-nearest neighbors with cognitive-inspired feature selection for high-dimensional data. *Big Data and Cognitive Computing*, *9*(8), 202. https://doi.org/10.3390/bdcc9080202

[60] Costa, V. G., & Pedreira, C. E. (2023). Recent advances in decision trees: An updated survey. *Artificial Intelligence Review*, *56*(5), 4765–4800. https://doi.org/10.1007/s10462-022-10275-5

[61] Sivaprasad, A., Reiter, E., Tintarev, N., & Oren, N. (2024). Evaluation of human-understandability of global model explanations using decision tree. In *Artificial Intelligence: ECAI 2023 International Workshops*, 43–65. https://doi.org/10.1007/978-3-031-50396-2_3

[62] Halabaku, E., & Bytyçi, E. (2024). Overfitting in machine learning: A comparative analysis of decision trees and random forests. *Intelligent Automation & Soft Computing*, *39*(6), 987–1006. https://doi.org/10.32604/iasc.2024.059429

[63] Chew, Y. J., Ooi, S. Y., Pang, Y. H., & Lim, Z. Y. (2025). Decision tree pruning with privacy-preserving strategies. *Electronics*, *14*(15), 3139. https://doi.org/10.3390/electronics14153139

[64] Shi, M., Hu, W., Li, M., Zhang, J., Song, X., & Sun, W. (2023). Ensemble regression based on polynomial regression-based decision tree and its application in the in-situ data of tunnel boring machine. *Mechanical Systems and Signal Processing*, *188*, 110022. https://doi.org/10.1016/j.ymssp.2022.110022

[65] Vapnik, V. N. (1995). *The nature of statistical learning theory* (1st ed.). USA: Springer. https://doi.org/10.1007/978-1-4757-2440-0

[66] Rodríguez-Pérez, R., & Bajorath, J. (2022). Evolution of support vector machine and regression modeling in chemoinformatics and drug discovery. *Journal of Computer-Aided Molecular Design*, *36*(5), 355–362. https://doi.org/10.1007/s10822-022-00442-9

[67] Wang, Q., Ma, Y., Zhao, K., & Tian, Y. (2022). A comprehensive survey of loss functions in machine learning. *Annals of Data Science*, *9*(2), 187–212. https://doi.org/10.1007/s40745-020-00253-5

[68] Bargam, B., Boudhar, A., Kinnard, C., Bouamri, H., Nifa, K., & Chehbouni, A. (2024). Evaluation of the support vector regression (SVR) and the random forest (RF) models accuracy for streamflow prediction under a data-scarce basin in Morocco. *Discover Applied Sciences*, *6*(6), 306. https://doi.org/10.1007/s42452-024-05994-z

[69] Jia, Y., Zhou, S., Wang, Y., Lin, F., & Gao, Z. (2025). A quadratic *v*-support vector regression approach for load forecasting. *Complex & Intelligent Systems*, *11*(1), 123. https://doi.org/10.1007/s40747-024-01730-7

[70] Smola, A. J., & Schölkopf, B. (2004). A tutorial on support vector regression. *Statistics and Computing*, *14*(3), 199–222. https://doi.org/10.1023/b:stco.0000035301.49549.88

[71] Breiman, L. (2001). Random forests. *Machine Learning*, *45*(1), 5–32. https://doi.org/10.1023/a:1010933404324

[72] Schauberger, G., Klug, S. J., & Berger, M. (2024). Random forests for the analysis of matched case–control studies. *BMC Bioinformatics*, *25*(1), 253. https://doi.org/10.1186/s12859-024-05877-5

[73] O’Connell, N. S., Jaeger, B. C., Bullock, G. S., & Speiser, J. L. (2025). A comparison of random forest variable selection methods for regression modeling of continuous outcomes. *Briefings in Bioinformatics*, *26*(2), bbaf096. https://doi.org/10.1093/bib/bbaf096

[74] Cappelli, F., Castronuovo, G., Grimaldi, S., & Telesca, V. (2024). Random forest and feature importance measures for discriminating the most influential environmental factors in predicting cardiovascular and respiratory diseases. *International Journal of Environmental Research and Public Health*, *21*(7), 867. https://doi.org/10.3390/ijerph21070867

[75] Yuan, X., Liu, S., Feng, W., & Dauphin, G. (2023). Feature importance ranking of random forest-based end-to-end learning algorithm. *Remote Sensing*, *15*(21), 5203. https://doi.org/10.3390/rs15215203

[76] Rezaei, N., & Jabbari, P. (2022). *Immunoinformatics of cancers: Practical machine learning approaches using R*. Netherlands: Elsevier.

[77] Abekoon, T., Sajindra, H., Rathnayake, N., Ekanayake, I. U., Jayakody, A., & Rathnayake, U. (2025). A novel application with explainable machine learning (SHAP and LIME) to predict soil N, P, and K nutrient content in cabbage cultivation. *Smart Agricultural Technology*, *11*, 100879. https://doi.org/10.1016/j.atech.2025.100879

[78] Barde, M. P., & Barde, P. J. (2012). What to use to express the variability of data: Standard deviation or standard error of mean? *Perspectives in Clinical Research*, *3*(3), 113–116. https://doi.org/10.4103/2229-3485.100662

[79] Hazra, A. (2017). Using the confidence interval confidently. *Journal of Thoracic Disease*, *9*(10), 4125–4130. https://doi.org/10.21037/jtd.2017.09.14

[80] Bolton, B. (2009). *Orthonasal, retronasal, and oral-cavity-only discrimination of vapor phase fatty acids*. Master's Thesis, Cornell University. http://ecommons.cornell.edu/bitstream/1813/13787/1/Bolton%2c%20Bryson.pdf

How to Cite: Palliyaguruge, M., Abekoon, T., Sajindra, H., Samarakoon, R., Rathnayake, N., & Rathnayake, U. (2026). Ensuring Turmeric Authenticity: A Web-Based AI Approach for Detecting Rice Flour Adulteration. *Journal of Data Science and Intelligent Systems*. https://doi.org/10.47852/bonviewJDSIS62027803